Defense Threat Reduction Agency
Research and Development
Counter WMD Technologies
Test Support Division
1680 Texas Street SE
Kirtland AFB, NM 87117-5669

DTRA TN-13-008

TECHNICAL NOTE

MICRONEEDLE DEVICE PROTOTYPE FINAL REPORT

May 2014

Authors: Philip Miller, Mathew Moorman, Susan Brozik, Thayne Edwards, David Wheeler, and Ronen Polsky
Sandia National Laboratories

Roger Narayan
University of North Carolina/North Carolina State University

REPORT DOCUMENTATION PAGE

Form Approved
OMB No. 0704-0188

1. REPORT DATE *(DD-MM-YYYY)*	**2. REPORT TYPE**	**3. DATES COVERED *(From-To)***
31 May 2014	Technical Note	16 July 2012 to 31 May 2014

4. TITLE AND SUBTITLE

Microneedle Device Prototype Final Report DTRA TN-13-008

5a. CONTRACT NUMBER

DTRA-10027-4390

5b. GRANT NUMBER

5c. PROGRAM ELEMENT NUMBER

6. AUTHOR (S)

Philip Miller, Mathew Moorman, Susan Brozik, Thayne Edwards, David Wheeler, and Ronen Polsky
Sandia National Laboratories

Roger Narayan
University of North Carolina/North Carolina State University

5d. PROJECT NUMBER

5e. TASK NUMBER

5f. WORK UNIT NUMBER

7. PERFORMING ORGANIZATION NAME(S) AND ADDRESS(ES)

Sandia National Laboratories
1515 Eubank SE
PO Box 5800
Albuquerque, NM 87123

8. **PERFORMING ORGANIZATION REPORT NUMBER**

DTRA TN-13-008

9. SPONSORING/MONITORING AGENCY NAME(S) AND ADDRESS(ES)

Technical Monitor: Bruce Hinds
Defense Threat Reduction Agency
8725 John J. Kingman Road
Fort Belvoir, VA 22060-6201

10. SPONSOR/MONITOR'S ACRONYM(S)

11. SPONSOR/MONITOR'S REPORT No.

12. DISTRIBUTION/AVAILABILITY STATEMENT

Distribution A: Approved for public release; distribution unlimited.

13. SUPPLEMENTARY NOTES

14. ABSTRACT

Real-time monitoring of an individual's physiological state without the constant presence of a healthcare professional would necessitate the construction of an autonomous remote diagnostic device that is capable of performing a wide range of diagnostic functions. For many applications, the immediate physiological state of a warfighter as he or she is continually exposed to diverse environments would require complex dynamic chemical processing scenarios that are capable of real-time readouts in order to maintain optimal health and effectiveness. The results presented here are an important proof-of-concept study to demonstrate how microneedles can be integrated with a microchip platform, complete with fluidic channels and electrode transducers, to extract interstitial fluid and monitor biologically important biomolecules toward a long-term remote diagnostic platform for defense of the warfighter. The project, part of a Defense Threat Reduction Agency research program, results consist of: (1) microneedle fabrication, (2) electrode array fabrication, (3) optimization of the electrode array for construction of an immunoassay for detection of myoglobin and troponin, and (4) integration of microneedles and the electrode array in a packaged chip.

15. SUBJECT TERMS

Microneedle Device Prototype Final Report DTRA TN-13-008, microneedle, voltammogram, carboxyl diazonium salt, e-Shell 300 resin, two-photon polymerization, myoglobin, troponin, sandwich antibody assay, capture antibody, detection antibody, gold electrodes, fluidic channel, real-time analytes, EDC/NHS chemistry

16. SECURITY CLASSIFICATION OF:			**17. LIMITATION OF ABSTRACT**	**18. NUMBER OF PAGES**	**19a. NAME OF RESPONSIBLE PERSON:**
					Bruce Hinds
a. REPORT	**b. ABSTRACT**	**c. THIS PAGE**	SAR	25	**19b. TELEPHONE NUMBER** *(include area code)*
UNCLASSIFIED	UNCLASSIFIED	UNCLASSIFIED			505-853-5722

Table of Contents

REPORT DOCUMENTATION PAGE ..... **ii**
Table of Contents ..... **iii**
List of Figures ..... **iv**
Acknowledgments ..... **v**
Executive Summary **1**
1.0 Introduction **2**
Background 2
Objectives 2
Security, Safety, and Environmental Considerations 2
Organization of This Report 2
2.0 Materials and Methods **3**
2.1 Cleaning Gold Arrays 3
2.2 Preparing and Depositing Carboxyl Diazonium Salts 3
2.3 Performing Immunoassay Procedure 4
3.0 Results and Discussion **5**
3.1 Fabricating Hollow Microneedles 5
3.2 Fabricating and Characterizing Electrode Array 7
3.3 Optimizing Electrode Array for Immunoassay 9
3.3.1 Characterizing Diazonium Deposition 10
3.3.2 Characterizing Immunoassay 12
3.3.3 Integrating Microneedles and Fluidic Chip 14
4.0 Conclusions **15**
Acronyms and Conversions **16**
List of Acronyms 16
Conversion Table 18
References **20**

List of Figures

Figure 3-1. Print screen of the STL file of a hollow microneedle design in Alibre (left) and a fabricated hollow microneedle made via two-photon method (right) 6
Figure 3-2. Influence of laser energy at the stage relative to the fabricated voxel size for e-Shell 300 6
Figure 3-3. Fabrication times for a hollow microneedle (450 × 1250 µm) with a variety of step heights between each fabricated layer 7
Figure 3-4. Optical image of electrode array, consisting of eight working electrodes, a counter electrode, and a reference electrode 8
Figure 3-5. Simultaneous electrochemical characterization of gold electrode (n = 8) array with oxide dielectric defined working electrodes with 1 mM $[Fe(CN)_6]^{3-}$ in 0.1 M potassium chloride (KCl) against an Ag/AgCl reference electrode and platinum wire counter electrode 9
Figure 3-6. Schematic of immunoassay protocol 10
Figure 3-7. Electrochemical deposition of in situ-generated carboxyl diazonium on a gold electrode against an Ag/AgCl reference electrode and a platinum wire counter electrode 11
Figure 3-8. Optimization of carboxyl diazonium deposition parameters determined by direct secondary antibody attachment of an HRP-labeled antibody, which was tested in a TMB conductivity solution 12
Figure 3-9. Calibration from immunoassay using varying concentrations of myoglobin 13
Figure 3-10. Calibration from immunoassay using varying concentrations of troponin I-T-C complex 13
Figure 3-11. Microneedle manifold with integrated electrode arrays and fluidic channel 14

Acknowledgments

This microneedle device prototype study was part of a Defense Threat Reduction Agency (DTRA) J9-CX research program.

Ronen Polsky of Sandia National Laboratories (SNL) prepared this report. Veronica Lopez, also of SNL, was the business manager. Bruce Hinds, DTRA Counter WMD Technology, was the program manager.

The Defense Threat Reduction Information Analysis Center provided organization and technical editing for this report.

Executive Summary

Real-time monitoring of an individual's physiological state without the constant presence of a healthcare professional would necessitate the construction of an autonomous remote diagnostic device that is capable of performing a wide range of diagnostic functions (Justino, Rocha-Santos, and Duarte 2010). For many applications, the immediate physiological state of a warfighter as he or she is continually exposed to diverse environments would require complex dynamic chemical-processing scenarios that are capable of real-time readouts in order to maintain optimal health and effectiveness. This project, part of a Defense Threat Reduction Agency (DTRA) J9-CX research program, seeks to answer these problems by combining in vivo microneedle platforms with multifunctional lab-on-chip electrode arrays that are capable of detecting a diverse number of relevant biomarkers.

Microneedles have been proven to be an effective and minimally invasive method for transdermal access of blood and interstitial fluid. Unlike conventional needles and lancets, microneedles cause minimal discomfort since they do not interact with deeper layers of the dermis, which are associated with sensation and pain. The most common use of microneedles has involved drug delivery applications (Gittard et al. 2010); however, it has been shown recently that they also can be used to extract fluid to detect physiological markers, such as glucose, lactate, and pH (Miller et al. 2012).

The results presented here are an important proof-of-concept study to demonstrate how microneedles can be integrated with a microchip platform, complete with fluidic channels and electrode transducers, to extract interstitial fluid and monitor biologically important biomolecules toward an on-body diagnostic platform for defense of the warfighter. The project results consist of: (1) microneedle fabrication, (2) electrode array fabrication, (3) optimization of the electrode array for construction of an immunoassay for detection of myoglobin and troponin, and (4) integration of microneedles and the electrode array in a packaged chip.

1.0 Introduction

Background

Real-time monitoring of an individual's physiological state without the constant presence of a healthcare professional would necessitate the construction of an autonomous remote diagnostic device that is capable of performing a wide range of diagnostic functions (Justino, Rocha-Santos, and Duarte 2010). For many applications, the immediate physiological state of a warfighter as he or she is continually exposed to diverse environments would require complex dynamic chemical-processing scenarios that are capable of real-time readouts in order to maintain optimal health and effectiveness.

Objectives

This project, part of a DTRA J9-CX research program, sought to answer these problems by combining in vivo microneedle platforms with multifunctional lab-on-chip electrode arrays that are capable of detecting a diverse number of relevant biomarkers. Microneedles have been proven to be an effective and minimally invasive method for transdermal access of blood and interstitial fluid. Unlike conventional needles and lancets, microneedles cause minimal discomfort since they do not interact with deeper layers of the dermis, which are associated with sensation and pain.

Security, Safety, and Environmental Considerations

All test results should be treated as Distribution A (approved for public release; distribution unlimited).

Organization of This Report

The introduction includes background material on this research and other considerations. Section 2.0 (Materials and Methods) presents the methodology, and Section 3.0 (Results and Discussion) presents the findings. Section 4.0 (Conclusions) summarizes overall conclusions.

2.0 Materials and Methods

2.1 Cleaning Gold Arrays

Gold (Au) electrode arrays had to be cleaned in order to remove residual material from the fabrication process since electrodes coming directly from the final fabrication step were not suitable for analytical electrochemical studies. A combination of a chemical treatment and an electrochemical treatment were used to clean the arrays. First, gold electrode arrays were sonicated in a solution of 50 mM potassium hydroxide (KOH) and 25% hydrogen peroxide (H_2O_2) for 10 min with solutions that were made fresh daily. One cyclic voltammogram was used as the electrochemical treatment in 50 mM KOH; scanning was performed from −200 mV to −1200 mV at 50 mV/s against a silver/silver chloride (Ag/AgCl) reference electrode and a platinum wire counter electrode. Electrodes were then washed with isopropanol, washed with deionized (DI) H_2O, and dried with a nitrogen stream. For electrodes that used Melinex windows, which were defined by laser cutting, the windows were applied after the cleaning steps were completed.

2.2 Preparing and Depositing Carboxyl Diazonium Salts

The gold array surfaces for attaching the primary antibody were modified by depositing a carboxyl diazonium salt (4-carboxylphenyl diazonium salt) using cyclic voltammograms for the deposition (Chung et al. 2012). The carboxyl diazonium molecules were created in situ by combining aqueous solutions of 10 mM p-aminophenyl propionic acid and 8 mM sodium nitrite ($NaNO_2$) in 0.5 M hydrochloric acid (HCl) for 10 min; this step was performed in the dark. The solution was then immediately deposited (releasing N_2 gas) on cleaned gold arrays by running cyclic voltammograms from 0.4 V to −0.6 V at 100 mV/s against an Ag/AgCl reference electrode and a platinum wire counter electrode. Once deposited, electrodes were cleaned by sonicating them in DI H_2O for 30 s, washing them with DI H_2O, and then drying them with nitrogen.

2.3 Performing Immunoassay Procedure

Gold arrays with the deposited carboxyl diazonium material were treated with an ethyl (dimethylaminopropyl) carbodiimide/N-hydroxysuccinimide (EDC/NHS) solution to activate the carboxylic acid (COOH) group in order to attach the primary antibody. An aqueous solution of 100 mM EDC and 25 mM NHS in a 10 mM 4-(2-hydroxyethyl)-1-piperazineethanesulfonic acid (HEPES) buffer (pH = 7.4) was applied to the surface of the gold arrays and left for 30 min. The solution was then washed off with 10 mM HEPES (pH = 7.4). A 2 ppm aqueous solution of the primary antibody in 10 mM HEPES (pH = 7.4) was applied to the surfaces of the electrodes. The appropriate primary antibodies for detecting myoglobin or troponin I, T, and C complex (troponin I-T-C) were used in this study. The electrodes were again rinsed with 10 mM HEPES buffer (pH = 7.4) and incubated in 1% bovine serum albumin (BSA) in 1× phosphate-buffered saline PBS (pH = 7.2) for 30 min to block unbound active sites. The electrodes were thoroughly washed with 1× PBS (pH = 7.2) and then treated with the desired concentration of protein in a 10 mM HEPES solution (pH = 7.4) for 1 hour. The electrodes were subsequently washed with 1× PBS (pH = 7.2). A 2 ppm solution of the secondary antibody in a 10 mM HEPES solution (pH = 7.4) was applied to the gold arrays, incubated for 1 hour, and washed with 1× PBS (pH = 7.2). Following a thorough washing of secondary-treated gold arrays, electrochemical detection was performed. A 3,3′–5,5′-tetramethylbenzidine (TMB) conductivity solution was applied to the electrodes, and a chronoamperometric scan was run at 0 V for 30 s against an Ag/AgCl reference electrode and a platinum wire counter electrode. For tests done to determine the optimal number of cyclic voltammograms for the diazonium deposition, the secondary antibody was directly attached to the activated COOH-terminated diazonium and then tested against the conductivity solution.

3.0 Results and Discussion

3.1 Fabricating Hollow Microneedles

Hollow microneedles were made using a laser direct-write system that uses the two-photon polymerization approach. First, substrates for the microneedles were made by molding a piece of polymethyl methacrylate (PMMA) (2 × 10 × 10 mm) with polydimethylsiloxane (PDMS), which was allowed to cure overnight. Then 250 µl of e-Shell 300, an acrylate-based material that is used to manufacture hearing aid shells, was poured into the mold and polymerized with a UV lamp for 20 min. Bores were created in the e-Shell 300 substrates to create a fluidic path between the hollow microneedles and the microfluidic chip. The bores were prepared by writing a 150 µm circle into the substrate with a CO_2 laser cutter. The exit bore was measured with an optical microscope to ensure that bores with an appropriate size were created; bores between 100 µm and 150 µm were considered to be suitable. Substrates were then washed with isopropanol to remove residual ablated material.

Microneedles were fabricated by creating a reservoir around the bore of the e-Shell 300 substrate with a parafilm spacer. The well was filled with e-Shell 300, and a glass coverslip was placed on top, minimizing inclusion of bubbles within the polymerization cell. A vacuum was pulled briefly at the backside of the substrate to introduce a small amount of resin into the bore. This approach enabled a portion of the microneedle to be written within the bore, which improved the strength of the needle–substrate interface and removed air bubbles around the substrate bore. The hollow microneedles were designed in Alibre or SolidWorks 3D design software (Dassault Systèmes, S. A., Vélizy, France), and the stereolithographic (STL) files were then read using GOLD3D custom laser direct software (Newport Spectra, Newport, California) (Figure 3-1). Completed microneedles were developed in isopropanol for 5 min. A vacuum was again pulled at the backside of the substrate to ensure that the bores were free of residual resin. Hollow microneedles were post-cured under a UV lamp to ensure complete polymerization.

The light source for fabricating the hollow microneedles was a titanium-sapphire (Ti:sapphire) laser that was operated at 800 nm wavelength, 150 fs pulse length, 80 MHz repetition rate, and 50–100 mW. The laser's beam was focused onto the sample with a 4× objective to increase the photon density and obtain two-photon polymerization of the resin.

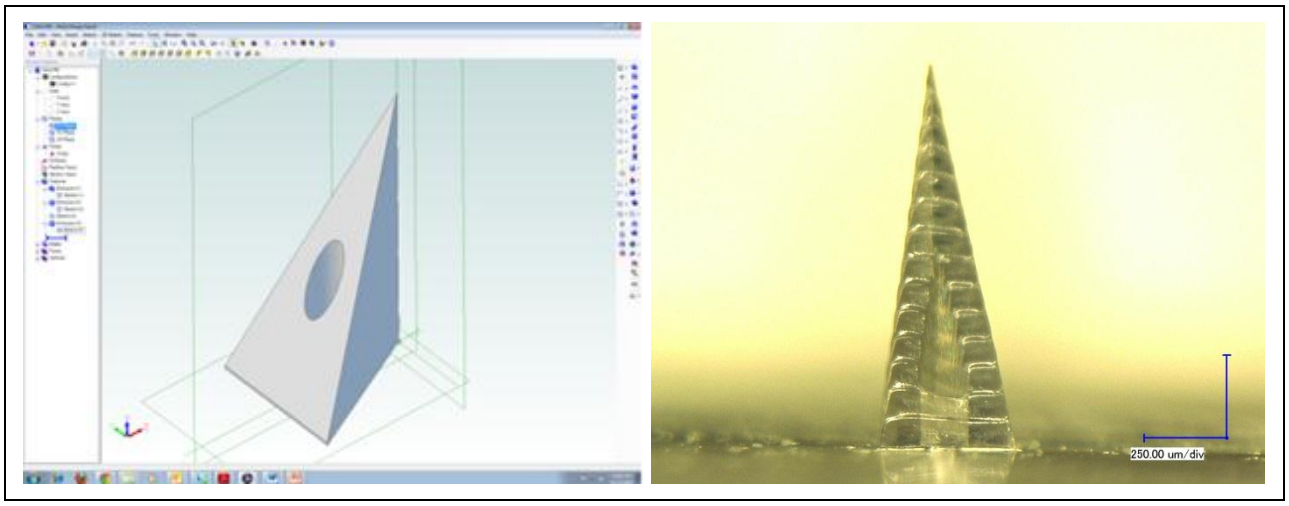

Figure 3-1. Print screen of the STL file of a hollow microneedle design in Alibre (left) and a fabricated hollow microneedle made via two-photon method (right)

Prior to fabricating a microneedle, the two-photon polymerization process for the e-Shell 300 resin and the objective was characterized. Figure 3-2 shows the length of the vertical voxel created at each tested energy. These results were used to optimize the step height between each layer, which affects fabrication time for the microneedle. Figure 3-3 shows fabrication times for the same hollow microneedle with dimensions of 500 µm by 1000 µm, in which only the spacing between each layer was altered. Microneedle fabrication parameters used in this study included a step height of 25 µm and a laser energy below 60 mW, due to the fact that laser power values above 60 mW were associated with over-polymerization and clogged hollow microneedle bores.

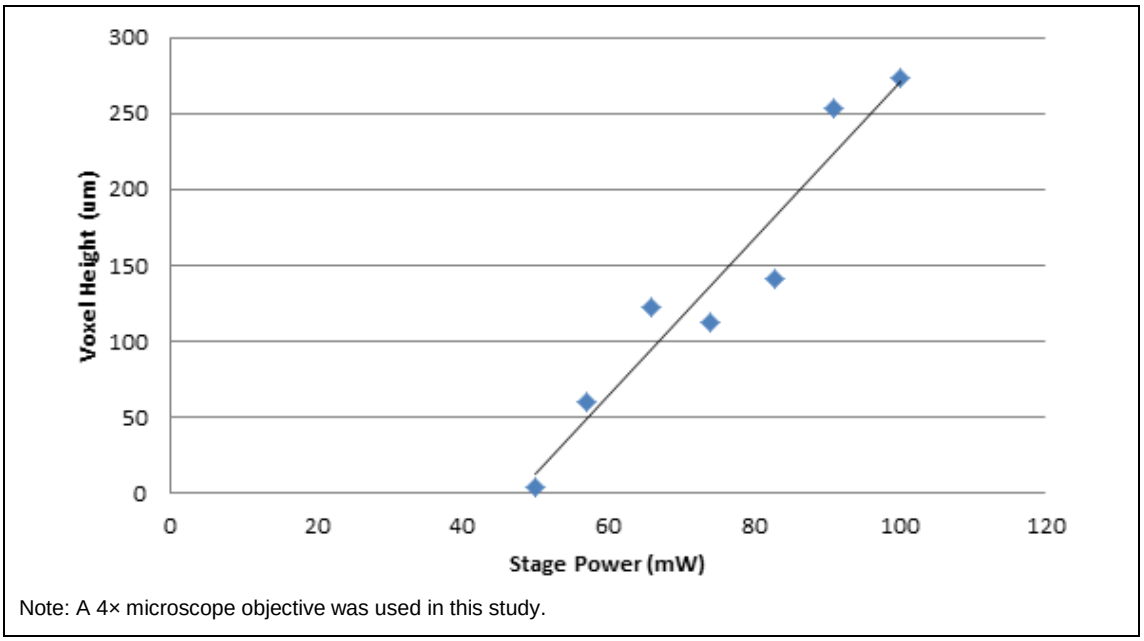

Note: A 4× microscope objective was used in this study.

Figure 3-2. Influence of laser energy at the stage relative to the fabricated voxel size for e-Shell 300

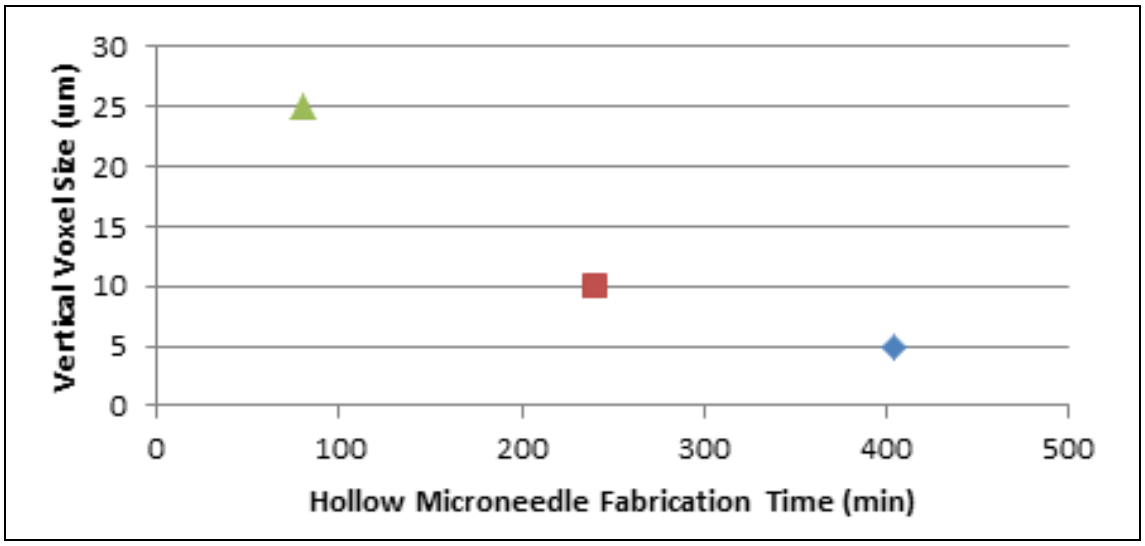

Figure 3-3. Fabrication times for a hollow microneedle (450 × 1250 µm) with a variety of step heights between each fabricated layer

3.2 Fabricating and Characterizing Electrode Array

An eight-element electrode array for integration with the microneedle array is presented in Figure 3-4. Six-inch diameter glass wafers were utilized as substrates for the electrode arrays. Standard photolithography techniques were used to pattern 150 Å chromium/3000 Å Au electrodes and contact pads. In order to precisely define the electrode surface area, a 2000 Å thick silicon nitride layer was deposited at 350°C over the entire device using plasma-enhanced chemical vapor deposition (PECVD). A photolithography step defined a precise opening over the dielectric layer, which measured 112 µm wide by 150 µm high. A sulfur hexafluoride (SF_6) plasma etch was then used to selectively remove the exposed silicon nitride until the Au layer underneath was reached. The magnified image in Figure 3-4 shows the 1120 × 150 µm Au working area, which is the only part of the electrode that was exposed to solution and was electrochemically active. Also shown are the counter and reference electrodes, which were patterned on the chip. The devices were then cut using a dicing saw. The final step was a 40 min oxygen plasma cleaning, which stripped fluorocarbon and photoresist residue from the chip surface.

Potential cycling in potassium ferricyanide ($K_3[Fe(CN)_6]$) mediator was then performed to assess electrode reproducibility and quality (Figure 3-5). Overlays of the electrodes' responses in ferricyanide solution show peak potential separation (ΔE_p) values of approximately 60 mV, with approximately 20 nA variations across the eight-element electrode array. This result indicates that the electrode response was highly reproducible and suitable for electrochemical measurements. The quasi-sigmoidal character of the voltammograms is indicative of the small working area of each electrode, resulting in hemispherical diffusion responses. Hemispherical diffusion is well known to be associated with high signal-to-noise responses.

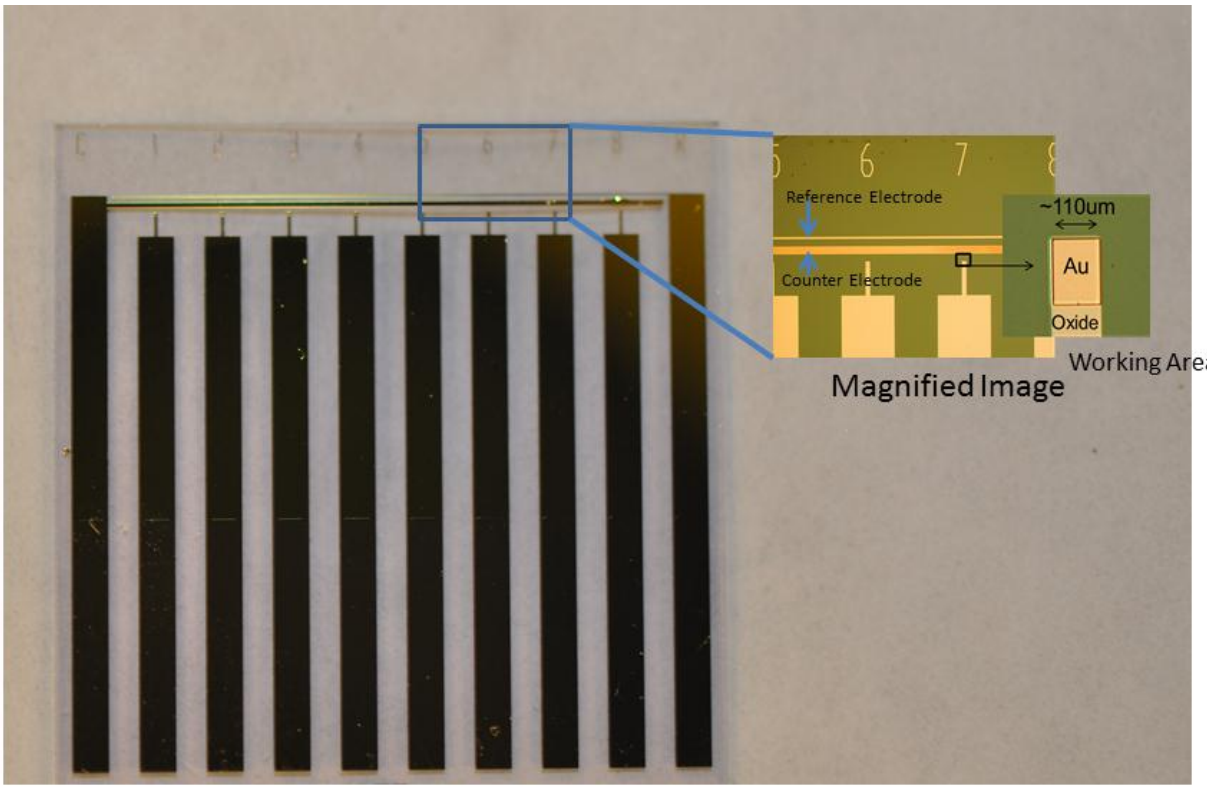

Note: Magnified images show exposed gold surrounded by a dielectric oxide passivation layer, which defines the working area that is electrochemically active (approximately 150 × 200 µm).

Figure 3-4. Optical image of electrode array, consisting of eight working electrodes, a counter electrode, and a reference electrode

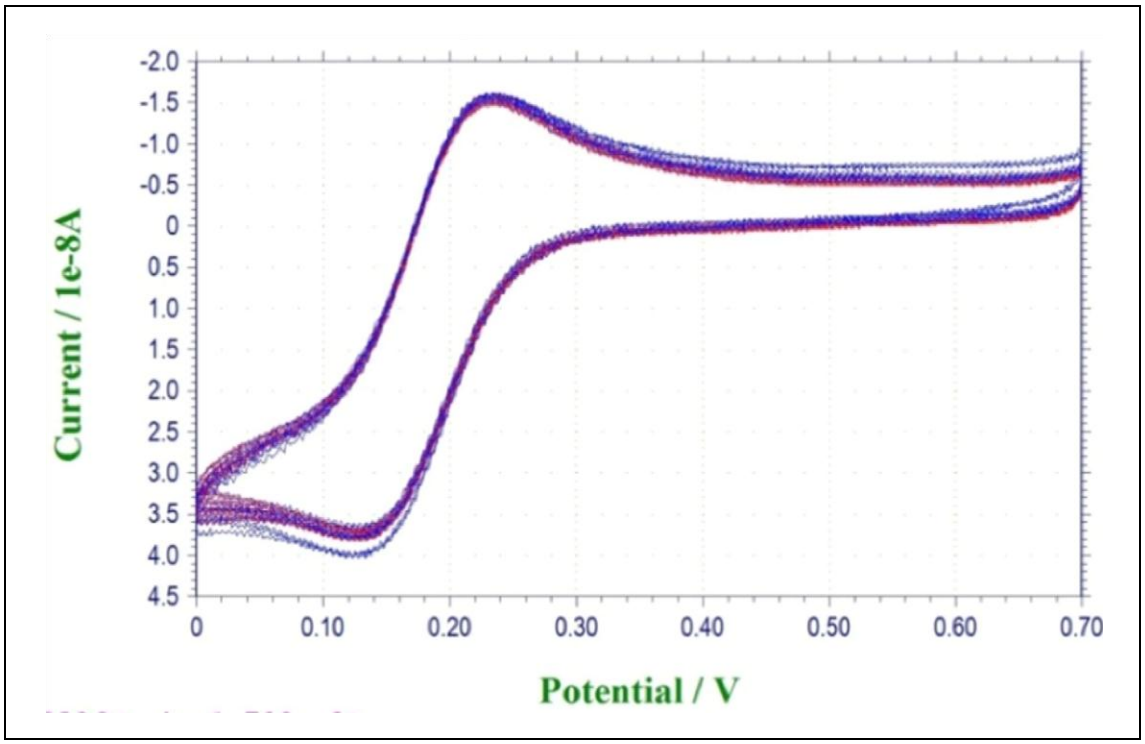

Figure 3-5. Simultaneous electrochemical characterization of gold electrode (n = 8) array with oxide dielectric defined working electrodes with 1 mM $[Fe(CN)_6]^{3-}$ in 0.1 M potassium chloride (KCl) against an Ag/AgCl reference electrode and platinum wire counter electrode

3.3 Optimizing Electrode Array for Immunoassay

The electrode array was optimized for immunoassays to detect either troponin or myoglobin. Troponin and myoglobin are used in clinical settings as biomarkers for detecting cardiac and skeletal muscle injuries, respectively. The approach used in this study was a sandwich antibody assay, consisting of a capture antibody and a secondary detection antibody labeled with a horseradish peroxidase (HRP) enzyme that catalyzes conversion of a TMB substrate to an electrochemically detectable product (Figure 3-6) (Polsky et al. 2008b). The electrodes were first modified with phenyl molecules to immobilize capture antibodies by electrochemical reduction from the corresponding phenyl diazonium molecules (Figure 3-6, inset) (Polsky et al. 2008a). This procedure is described in detail in Section 2.2.

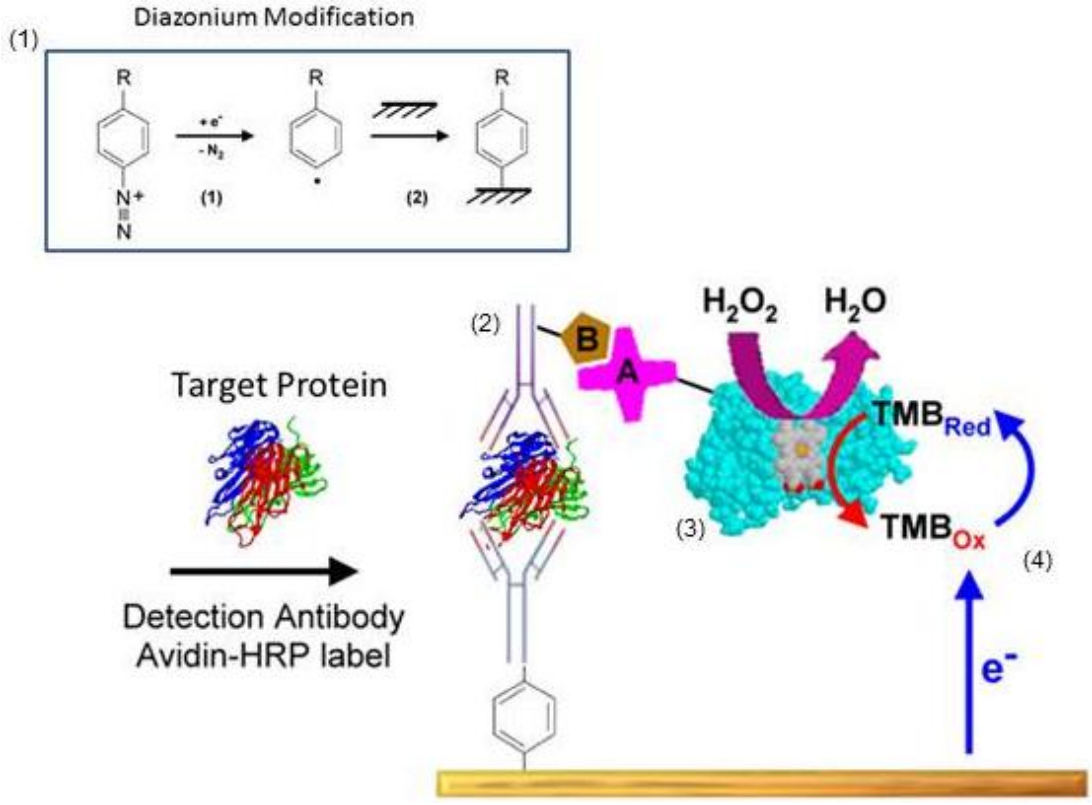

Note: Immunoassay protocol consists of (1) immobilization of capture antibody, (2) capture of target protein, (3) immobilization of HRP-labeled secondary antibody, and (4) catalytic turnover of TMB substrate to produce TMB_{Ox} and an electrochemical signal.
Note: The inset shows the process of electrochemically immobilizing a phenyl molecule used to conjugate a capture antibody from corresponding diazonium salt.

Figure 3-6. Schematic of immunoassay protocol

3.3.1 Characterizing Diazonium Deposition

Electrochemical deposition of carboxyl diazonium on gold electrodes resulted in an irreversible reduction wave on the first scan of a cyclic voltammogram, as shown in Figure 3-7. Reduction peaks at approximately 0 V and –400 mV are indicative of the in situ-generated diazonium reduction at different crystal planes on the gold electrodes. Subsequent voltammograms showed no reduction waves due to electrode passivation from phenyl radical grafting, a process that is commonly observed during deposition of phenyl diazonium molecules.

Carboxyl diazonium deposition parameters were optimized to determine the number of cyclic voltammograms necessary for the largest and most consistent current responses from directly conjugating the HRP-labeled antibody and measuring enzymatic activity by means of electrochemical transduction. Cleaned electrodes were deposited with the in situ carboxyl diazonium at 1, 5, or 10 cyclic voltammograms. The secondary antibody was then attached via EDC/NHS chemistry and tested against the TMB conductivity solution. Electrodes with 1, 5, and 10 cyclic voltammograms of diazonium deposition exhibited an average current response of 63 nA, 74 nA, and 123 nA, respectively (Figure 3-8). Electrodes that were modified using 10 cyclic voltammograms of diazonium deposition produced the largest magnitude and most consistent reduction signals; therefore, electrodes modified using 10 cyclic voltammograms were used for all further depositions.

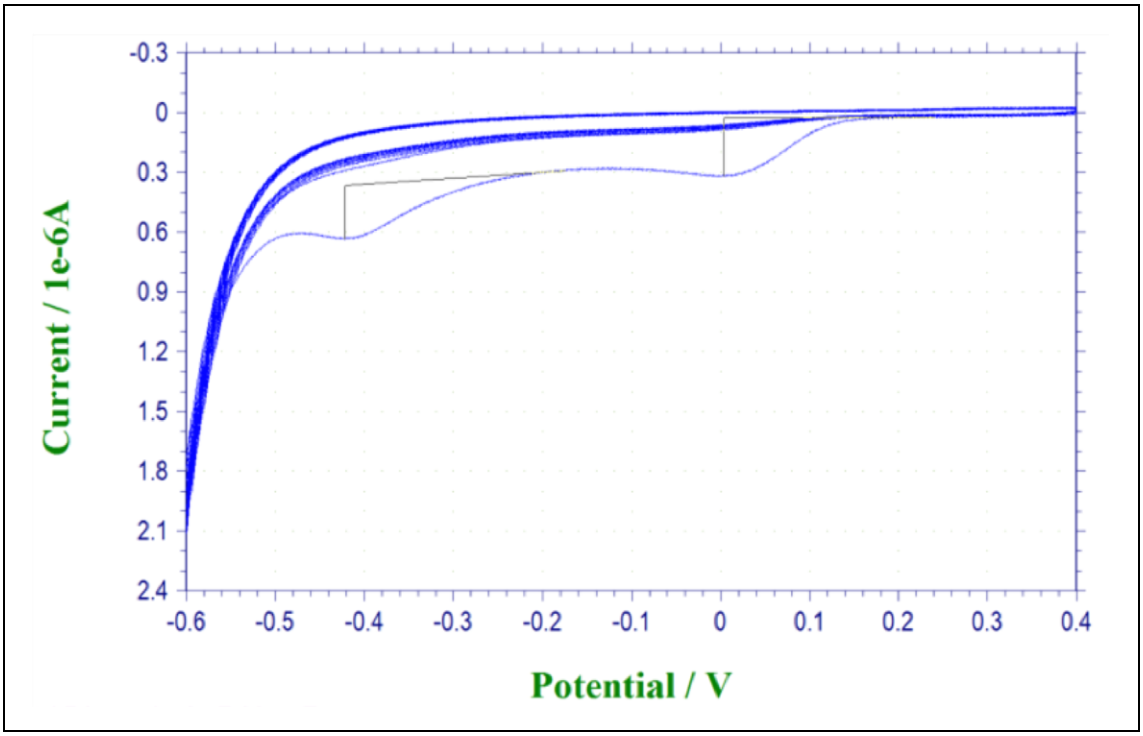

Figure 3-7. Electrochemical deposition of in situ-generated carboxyl diazonium on a gold electrode against an Ag/AgCl reference electrode and a platinum wire counter electrode

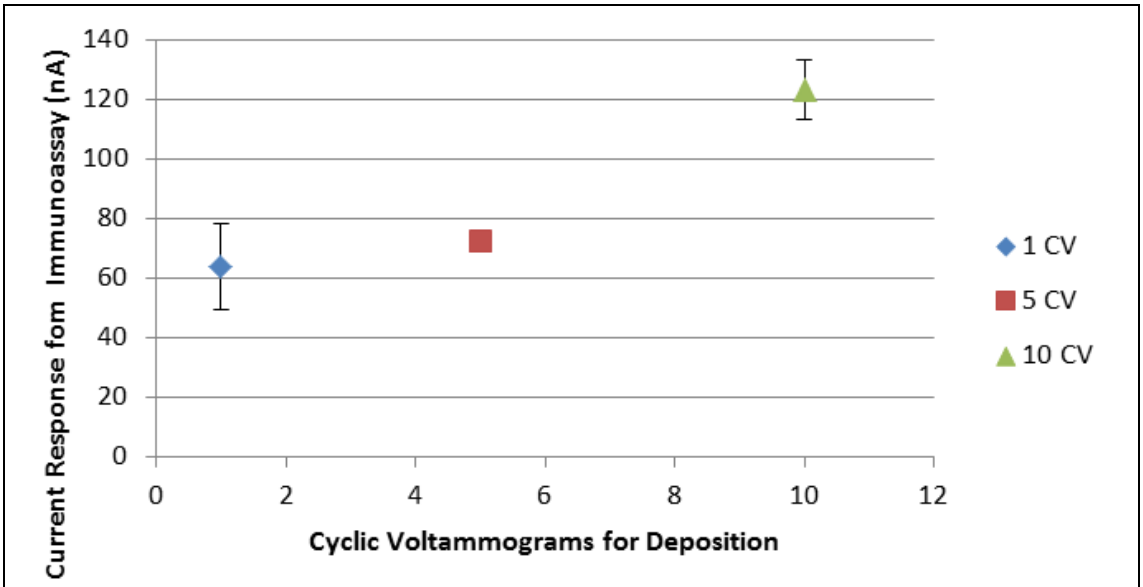

Note: Error bars for the 5CV deposition are hidden by the marker.

Figure 3-8. Optimization of carboxyl diazonium deposition parameters determined by direct secondary antibody attachment of an HRP-labeled antibody, which was tested in a TMB conductivity solution

3.3.2 Characterizing Immunoassay

Sandwich immunoassays consisted of exposure to the target protein followed by an HRP-labeled capture antibody treatment (Section 2.3). A fast steady-state current was achieved upon chronoamperometric biasing of the electrode to 0 V, corresponding to the electroreduction of the oxidized TMB mediator. After exposure to varying protein concentrations, the sensor response was obtained 5 s after the potential step. Calibration curves generated for myoglobin and troponin I-T-C complex are presented in Figure 3-9 and Figure 3-10, respectively. A dependence of signal on concentration was observed for both proteins between 100 ppb and 1000 ppb, demonstrating that this technique is suitable for quantitative detection. Measurements were averaged from eight electrodes for each data point.

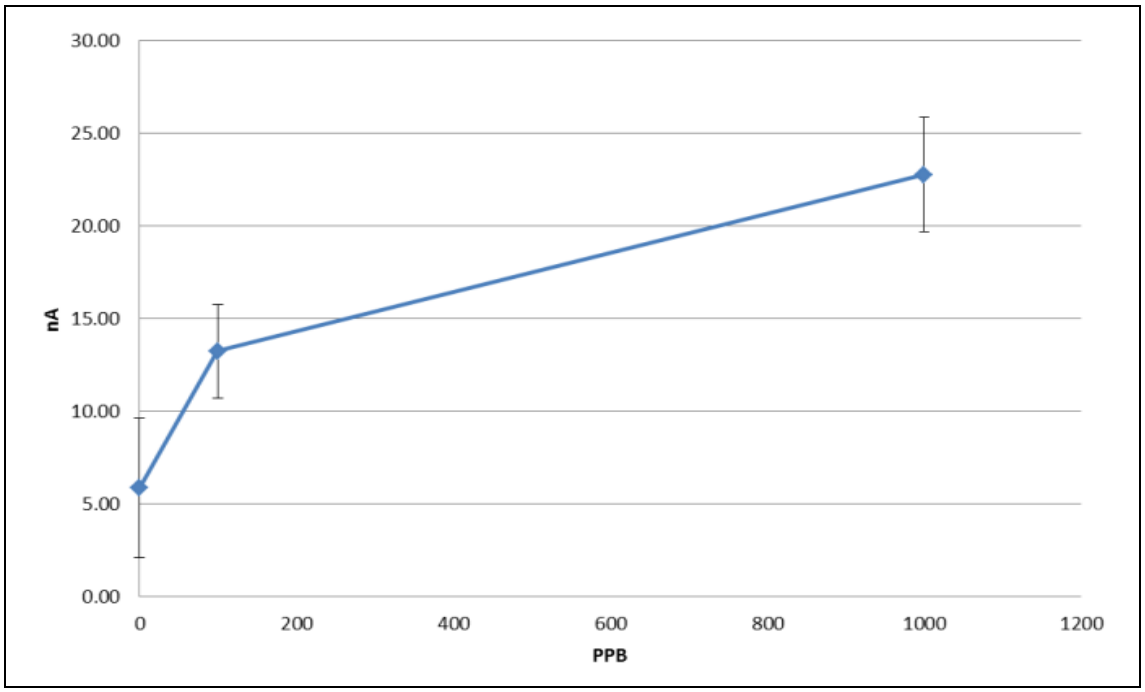

Figure 3-9. Calibration from immunoassay using varying concentrations of myoglobin

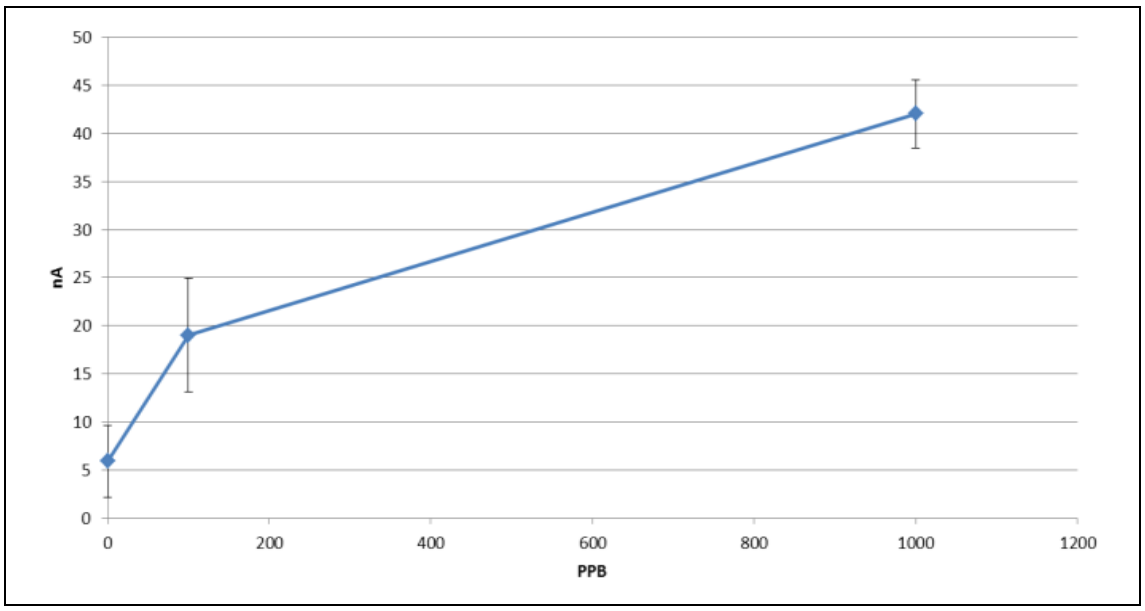

Figure 3-10. Calibration from immunoassay using varying concentrations of troponin I-T-C complex

3.3.3 Integrating Microneedles and Fluidic Chip

A microfluidic manifold was constructed from acrylic sheets and medical-grade Mylar adhesives using a precision cutting laser. The acrylic sheets were typically 2 mm thick, though thinner or thicker sheets could be used depending on application, mechanical robustness associated with intended function, and form factor. Medical-grade Mylar adhesive was chosen because it is frequently used in the construction of commercial bioassay devices; it has demonstrated low outgassing, low chemical leaching, and biocompatibility. Each of these materials was cut with a laser and sequentially assembled on a jig to create complex fluidic networks, with lateral flow channels being formed in the adhesive layers and connecting vias being formed in the acrylic sheet. Once the layers were stacked and assembled, they were pressed together for 2 min at 500 psi to assure good adhesion of the laminate layers. The design featured one acrylic layer and two adhesive layers, with the bottom adhesive layer forming the flow channel on the surface of the electrochemistry sensing chip and the top adhesive layer sealing the microneedles to the laminate cartridge. In order to provide for external fluid connections, a conventional Viton rubber O-ring (size 001) was enclosed within the cartridge. Inserting 0.03125 in. tubing into these captured O-rings created a fluid-tight seal and allowed pressure to either inject or draw fluid through the microneedle array. The final integrated package is shown in Figure 3-11.

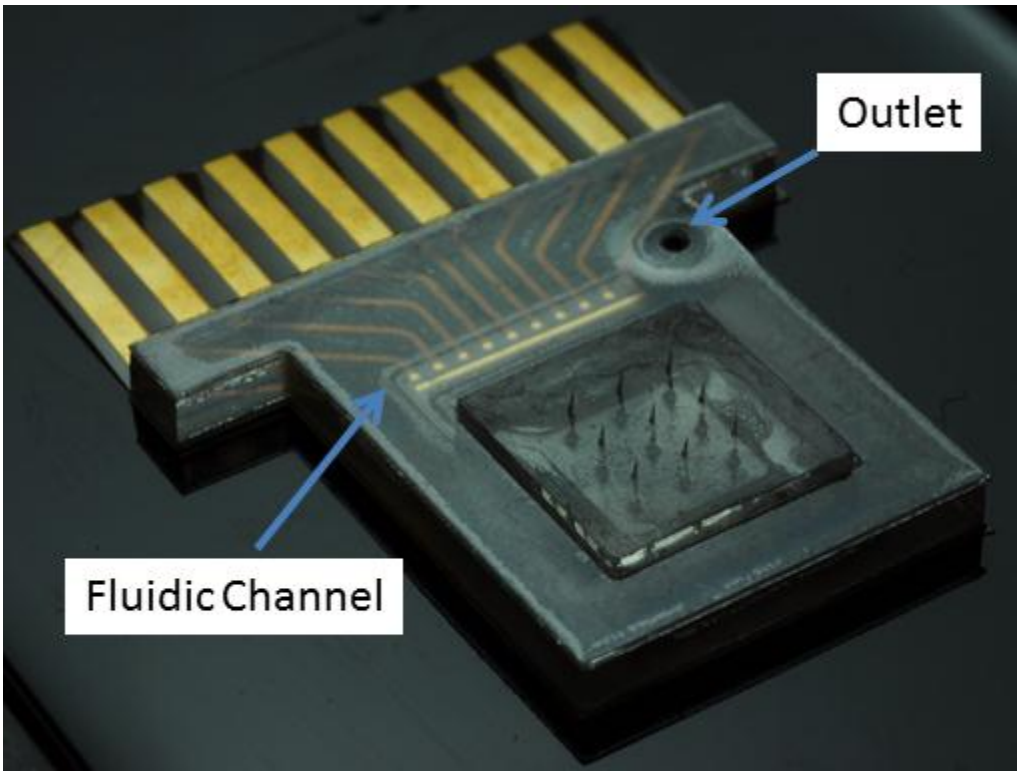

Figure 3-11. Microneedle manifold with integrated electrode arrays and fluidic channel

4.0 Conclusions

In conclusion, a hollow microneedle manifold was developed, complete with integrated electrode arrays and a fluidic channel. An eight-channel electrode array was fabricated using photolithographic patterning and dielectric insulating layers to expose a 112 µm wide by 150 µm high Au working area, which was used as an electrochemical transducer. Potassium ferricyanide cycling was used to characterize the response over the eight working electrodes, which were shown to be highly reproducible and suitable for electrochemical measurements. The electrodes were then modified using potentially addressable diazonium chemistry to immobilize a capture antibody, allowing for different labels to be put down on closely spaced electrodes for multianalyte detection. The electrodes were optimized subsequently to detect target proteins—troponin, a cardiac injury marker, and myoglobin, a skeletal injury marker—using an electrochemical sandwich immunoassay protocol. The resulting chip was packaged using plastic laminate technology with a fluidic channel that could access the microneedles and flow solution over the electrode array. This type of device is a significant advancement toward an autonomous microneedle platform, which is capable of transdermally accessing interstitial fluid and performing real-time and repeated measurements for a variety of physiologically relevant analytes.

Acronyms and Conversions

This section includes the list of acronyms and the conversion table.

List of Acronyms

Acronyms	
Ag/AgCl	silver/silver chloride
Au	gold
BSA	bovine serum albumin
carboxyl diazonium salt	4-carboxylphenyl diazonium salt
COOH	carboxylic acid
DI	deionized
DTRA	Defense Threat Reduction Agency
EDC/NHS	ethyl (dimethylaminopropyl) carbodiimide/ N-hydroxysuccinimide
$Fe(CN)_6$	ferricyanide
$[Fe(CN)_6]^{3-}$	ferricyanide ion
H_2O_2	hydrogen peroxide
HEPES	4-(2-hydroxyethyl)-1-piperazineethanesulfonic acid
HRP	horseradish peroxidase
$K_3[Fe(CN)_6]$	potassium ferricyanide
KCl	potassium chloride
KOH	potassium hydroxide
$NaNO_2$	sodium nitrite
PBS	phosphate-buffered saline
PDMS	polydimethylsiloxane
PECVD	plasma-enhanced chemical vapor deposition
PMMA	polymethyl methacrylate
ppb	parts per billion

Acronyms	
ppm	parts per million
SF_6	sulfur hexafluoride
Ti:sapphire	titanium-sapphire
TMB	tetramethylbenzidine
troponin I-T-C	troponin I, troponin T, and troponin C protein complex

Conversion Table

This table includes conversion factors for changing US customary measures to metric (SI) units of measurement, and vice versa.

Multiply US ———> by Conversion ———> To Get SI

To Get US ———> by Conversion ———> Divide SI

US Measurement	Conversion	SI Measurement
angstrom	$1.000\ 000 \times 10^{-10}$	meters (m)
atmosphere (normal)	$1.013\ 250 \times 10^{2}$	kilo pascal (kPa)
bar	$1.000\ 000 \times 10^{2}$	kilo pascal (kPa)
barn	$1.000\ 000 \times 10^{-28}$	meter^2 (m^2)
British thermal unit (thermochemical)	$1.054\ 350 \times 10^{3}$	joule (J)
calorie (thermochemical)	4.184 000	joule (J)
cal (thermochemical/cm^2)	$4.184\ 000 \times 10^{-2}$	mega joule /m^2 (MJ/m^2)
curie	$3.700\ 000 \times 10^{1}$	giga becquerel (Gbq)*
degree (angle)	$1.745\ 329 \times 10^{-2}$	radian (rad)
degree Fahrenheit	$T_K = (T_F + 459.67)/1.8$	degree Kelvin (°K)
electron volt	$1.602\ 177 \times 10^{-19}$	joule (J)
erg	$1.000\ 000 \times 10^{-7}$	joule (J)
erg/second	$1.000\ 000 \times 10^{-7}$	watt (W)
foot	$3.048\ 000 \times 10^{-1}$	meter (m)
foot-pound-force	1.355 818	joule (J)
gallon (US liquid)	$3.785\ 412 \times 10^{-3}$	meter^3 (m^3)
inch	$2.540\ 000 \times 10^{-2}$	meter (m)
jerk	$1.000\ 000 \times 10^{9}$	joule (J)
joule/kilogram (J/kg) radiation dose absorbed	1.000 000	Gray (Gy)**
kilotons	4.183	terajoules
kip (1000 1bf)	$4.448\ 222 \times 10^{3}$	newton (N)

US Measurement	Conversion	SI Measurement
kip/inch^2 (ksi)	6.894 757 × 10^3	kilo pascal (kPa)
ktap	1.000 000 × 10^2	newton-second/m^2 (N•s/m^2)
micron	1.000 000 × 10^{-6}	meter (m)
mil	2.540 000 × 10^{-5}	meter (m)
mile (international)	1.609 344 × 10^3	meter (m)
ounce	2.834 952 × 10^{-2}	kilogram (kg)
pound-force (lbf avoirdupois)	4.448 222	newton (N)
pound-force inch	1.129 848 × 10^{-1}	newton-meter (N•m)
pound-force/inch	1.751 268 × 10^2	newton/meter (N/m)
pound-force/foot^2	4.788 026 × 10^{-2}	kilo pascal (kPa)
pound-force/inch^2 (psi)	6.894 757	kilo pascal (kPa)
pound-mass (lbm avoirdupois)	4.535 924 × 10^{-1}	kilogram (kg)
pound-mass-foot^2 (moment of inertia)	4.214 011 × 10^{-2}	kilogram-meter^2 (kg•m^2)
pound-mass/foot^3	1.601 846 × 10^1	kilogram/meter^3 (kg/m^3)
rad (radiation dose absorbed)	1.000 000 × 10^{-2}	Gray (Gy)**
rem (roentgen equivalent man)	1.000 000 × 10^{-2}	Sievert (Sv)***
roentgen	2.579 760 × 10^{-4}	coulomb/kilogram (C/kg)
shake	1.000 000 × 10^{-10}	second (s)
slug	1.459 390 × 10^1	kilogram (kg)
torr (mm Hg, 0º C)	1.333 22 × 10^{-1}	kilo pascal (kPa)

* The becquerel (Bq) is the SI unit of radioactivity; 1 Bq = 1 event/s.
** The Gray (GY) is the SI unit of absorbed radiation.
*** The Sievert (SV) is the SI unit of dose equivalent.

References

Chung, D. J., et al. 2012. "One-Step Modification of Various Electrode Surfaces Using Diazonium Salt Compounds and the Application of This Technology to Electrochemical DNA (E-DNA) Sensors." *Electrochimica Acta*, 76:394–403. http://www.sciencedirect.com/science/article/pii/S0013468612008109.

Gittard, S. D., A. Ovsianikov, B. N. Chichkov, A. Doraiswamy, and R. J. Narayan. 2010. *Exp. Opin. Drug Deliv.*, 513.

Justino, C. I. L., T. A. Rocha-Santos, and A. C. Duarte. 2010. *Trends Analyt. Chem.*, 29:1172.

Miller, P. R., S. A. Skoog, T. L. Edwards, D. M. Lopez, D.R. Wheeler, D.C. Arango, X. Xiao, S. M. Borozik, J. Wang, R. Polsky, and R. J. Narayan. 2012. *Talanta*, 88:739.

Polsky, R., J. C. Harper, D. R. Wheeler, and S. M. Brozik. 2008a. *Electroanalysis*, 20:671.

Polsky, R., J. C. Harper, D. R. Wheeler, S. M. Dirk, D. C. Arango, and S. M. Brozik. 2008b. *Biosens. Bioelec.*, 23:757.